PAPER

Accurate Height Change Estimation Method Using Phase Interferometry of Multiple Band-Divided SAR Images

Ryo NAKAMATA[†], ***Member***, **Ryo OYAMA**[††], ***Student Member***, **Shouhei KIDERA**[††a)], ***and*** **Tetsuo KIRIMOTO**[††], ***Members***

SUMMARY Synthetic aperture radar (SAR) is an indispensable tool for low visibility ground surface measurement owing to its robustness against optically harsh environments such as adverse weather or darkness. As a leading-edge approach for SAR image processing, the coherent change detection (CCD) technique has been recently established; it detects a temporal change in the same region according to the phase interferometry of two complex SAR images. However, in the case of general damage assessment following an earthquake or mudslide, the technique requires not only the detection of surface change but also an assessment for height change quantity, such as occurs with a building collapse or road subsidence. While the interferometric SAR (InSAR) approach is suitable for height assessment, it is basically unable to detect change if only a single observation is made. To address this issue, we previously proposed a method of estimating height change according to phase interferometry of the coherence function obtained by dual band-divided SAR images. However, the accuracy of this method significantly degrades in noisy situations owing to the use of the phase difference. To resolve this problem, this paper proposes a novel height estimation method by exploiting the frequency characteristic of coherence phases obtained by each SAR image multiply band-divided. The results obtained from numerical simulations and experimental data demonstrate that our proposed method offers accurate height change estimation while avoiding degradation in the spatial resolution.

key words: *synthetic aperture radar (SAR), coherent change detection (CCD), multiply band-divided SAR images, height change estimation*

1. Introduction

A high-resolution microwave imaging technique, especially for synthetic aperture radar(SAR), is one of the most useful tools for measuring terrain surface, because it is applicable to surface imaging in adverse weather or darkness [1], [2]. In recent years, as the one of the most cutting-edge derivative techniques of SAR, coherent change detection (CCD) has been intensively developed [3], [4]. The concept of CCD is simply based on the local spatial correlation between sequential complex SAR images obtained through observation of the same region at different times. However, traditional CCD techniques were designated to detect surface change, and so fail to address height change measurements. Such information of height change is needed to judge if a road is suitable for motor vehicle use following a disaster. A classical but powerful tool for measuring height is interferometric SAR (InSAR): InSAR is based on the phase interferometry of plural SAR images obtained from different scanning orbits [4]. There are various derivation techniques for InSAR, such as the polarimetric approach (PolInSAR) [5], which classifies a target according to the characteristic of the polarization of the received signal, and a method [6], based on the differential SAR Interferometry (DinSAR), that employs the likelihood function and frequency diversity to unwrap a phase distribution. However, this type of technique has the significant drawback that the obtained height is relative to a reference point owing to phase wrapping, and thus, in the case of great height changes in spatially narrow areas, this method fails to output the correct relative height distribution. In addition, the InSAR techniques described above have been developed as a height estimation method and are not capable of detecting change because it assumes a temporal invariance of target surface.

To address such problem, we have already proposed a method of estimating height change with a CCD model [7], namely, the InSAR model with zero baseline length. This method employs dual band-divided SAR images to resolve the ambiguity inherent in height change estimation. In this method, each height change can be calculated using the phase difference between the two coherence functions obtained from the dual band-divided SAR images. However, if the signal to noise ratio (SNR) is low, the accuracy of this method is severely degraded in terms of height change because the phase difference approach is generally too sensitive to the fluctuation caused by random noises. Thus, to maintain a certain level of accuracy, the method requires spatial averaging over a large area, which degrades the spatial resolution of the height change assessment. In other words, the conventional method has an inherent trade-off between the accuracy and spatial resolution of the height change estimation.

As a solution to the above difficulty, this paper proposes a novel height estimation method for the CCD model; it employs multiple band-divided SAR images and their coherence functions with phases. To accurately reconstruct the height change even if the observed phase fluctuates due to random noise, this method focuses on the phase characteristic for each center frequency and resolves the ambiguity by employing a multiple non-linear regression scheme. In other words, the proposed method enhances robustness against phase fluctuation by employing not the spatial averaging, but a type of frequency averaging scheme. This

Manuscript received August 19, 2013.
Manuscript revised December 27, 2013.

[†]The author is with the Software Development Section, Sigmatron Co., Ltd., Tokyo, 103-0023 Japan.
[††]The authors are with the Graduate School of Informatics and Engineering, The University of Electro-Communications, Chofushi, 182-8585 Japan.
a) E-mail: kidera@ee.uec.ac.jp

DOI: 10.1587/transcom.E97.B.1205

method is notable in that it can maintain the accuracy of height change estimation without degrading the spatial resolution of the estimation, and is also suitable for detecting a temporal change of target surface.

This paper is organized as follows. Section 2 introduces the observation model assuming a 1/100 downscaled model of the actual X-band radar system. Section 3 presents the conventional method used for height change estimation, and states its problem. Section 4 describes the basic concept and detailed methodology of the proposed method. Finally, performance evaluations are carried out in a numerical simulation and experiment in Sect. 5. The results demonstrate that the proposed method accurately estimate height change without degrading the spatial resolution, even in noisy or actual situations.

2. System Model

Figure 1 shows the observation geometry. It assumes that there is a target with a rough surface around the $z = 0$ plane, and that the propagation speed of the microwave is a known constant. A monostatic radar is assumed, and a set of scans is made along the line of $z = \mathrm{z}_0$, $y = 0$ by a transmitting and receiving antenna, located at $(x, 0, \mathrm{z}_0)$. The off-nadir angle is denoted θ. Each antenna receives the complex-valued reflection signal $S(x; f)$ at each frequency f, where the signal is swept in a finite frequency range with the pulse compression technique. The height of the target surface is changed between the first and second observations. $s_1(x, y)$ and $s_2(x, y)$ denote the complex SAR images of the target focused on the $z = 0$ plane before and after surface changes, respectively. The coherence function $\gamma(x, y)$ between the two SAR images is defined as [4]

$$\gamma(x_i, y_j) = \frac{\sum_{m,n=-L/2}^{L/2} s_1^*\left(x_{i,m}, y_{j,n}\right) s_2\left(x_{i,m}, y_{j,n}\right)}{\sqrt{\sum_{m,n=-L/2}^{L/2} \left|s_1\left(x_{i,m}, y_{j,n}\right)\right|^2} \sqrt{\sum_{m,n=-L/2}^{L/2} \left|s_2\left(x_{i,m}, y_{j,n}\right)\right|^2}}, \tag{1}$$

where $x_{i,m} = x_i + m\Delta l$ and $y_{j,n} = y_j + n\Delta l$, and Δl is the sampling interval along the x and y axes of the SAR image. * denotes a complex conjugate and L determines the correlation length for the coherence estimation. Under the assumption that the target surface moves along the z axis, the height change $\Delta z(x, y)$ can be calculated from the phase of coherence function $\gamma(x, y)$,

$$\Delta z(x, y) \approx -\frac{\mathrm{c}}{4\pi f_\mathrm{c} \cos\theta(x, y)} \psi(x, y), \tag{2}$$

where $\psi(x, y)$ denotes the phase of $\gamma(x, y)$ and f_c is the center frequency of the transmitted signal. $\theta(x, y)$ is the off-nadir angle averaged over all antenna locations of observations. Figure 2 shows the geometrical relationship between the height change and off-nadir angle. Note that, there should be ambiguity in determining the actual height change due to the phase of the coherence function. The amount of this ambiguity for the center frequency f_c is calculated as

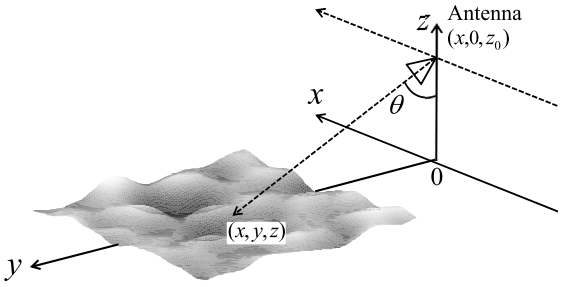

Fig. 1 Observation geometry.

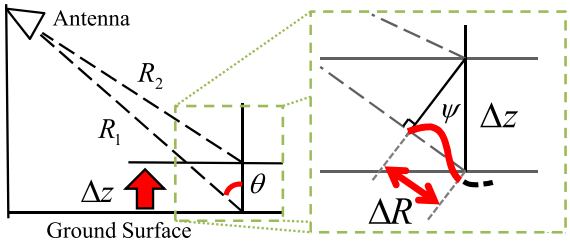

Fig. 2 Geometrical relationship between the phase difference and height change amount.

$$\Delta z_\mathrm{amb} = \frac{\mathrm{c}}{2f_\mathrm{c} \cos\theta(x, y)}. \tag{3}$$

3. Conventional Method

As one approach for estimating the height change using the CCD model, this section introduces a representative [7] of the conventional methods; the method is based on the phase interferometry of the coherence function. It should be noted that there is an essential problem relating to height ambiguity in using a phase interferometer as seen in Eq. (3). As a solution for avoiding the ambiguity, the conventional method [7] employs two coherence functions defined using the dual band-divided SAR imagery with the same bandwidth but different center frequencies. First, the two complex SAR images are generated from the dual band-divided received signal, where each center frequency is different. Each phase of the coherent function calculated from the SAR images taken before and after surface change, is determined as $\psi_1(x, y)$ and $\psi_2(x, y)$. The amount of height change then is calculated as

$$\Delta\hat{z}_\mathrm{conv}(x, y) = -\frac{\mathrm{c}}{4\pi\Delta f_\mathrm{c} \cos\theta(x, y)} \Delta\psi(x, y), \tag{4}$$

where $\Delta\psi(x, y) = \psi_1(x, y) - \psi_2(x, y)$, and Δf_c denotes the center frequency difference.

Step 1) Received signals are divided into two frequency bands with different center frequencies.

Step 2) SAR images taken before and after the change event are generated in each frequency band as $s_1(x, y; f_{\mathrm{c},n})$ and $s_2(x, y; f_{\mathrm{c},n})$, where $n = 1, 2$.

Step 3 Position adjustment between $s_1(x, y; f_{\mathrm{c},n})$ and $s_2(x, y; f_{\mathrm{c},n})$ is carried out, so that the output of local

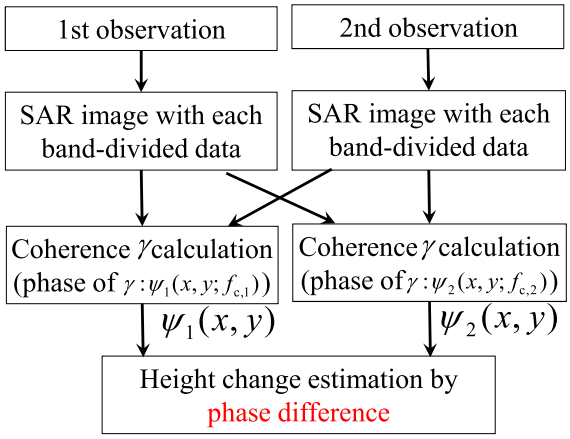

Fig. 3 Flowchart of the conventional method.

cross-correlation of these two images becomes maximum. The window size of the local cross-correlation is empirically determined.

Step 4) Coherence function $\gamma_n(x,y;f_{c,n})$ is calculated from $s_1(x,y;f_{c,n})$ and $s_2(x,y;f_{c,n})$, and the phase of $\gamma_n(x,y;f_{c,n})$ as $\psi_n(x,y;f_{c,n})$ is also calculated.

Step 5) The height change is calculated using Eq. (4).

Figure 3 shows a flowchart illustrating the conventional method. In this case, the ambiguity of the height estimation is expanded using the frequency shift as

$$\Delta z_{\mathrm{amb}} = \frac{\mathrm{c}}{2\Delta f_{\mathrm{c}} \cos\theta(x,y)}. \tag{5}$$

Note that, Step 3) compensates a position gap between $s_1(x,y)$ and $s_2(x,y)$ due to layover caused by height change. According to the above discussion, the maximum range of the height estimation is extended as Δf_{c} decreases. However, in the case of a smaller Δf_{c}, the height estimation itself is more sensitive to the phase fluctuations caused by the noise or other interfering components. To reduce this sensitivity, the conventional method must average $\Delta\psi$ over a large part of the target region, which degrades the spatial resolution. On the other hand, to maintain the spatial resolution, while this method needs a sufficient bandwidth, it enhances the sensitivity to the noise due to smaller difference of the center frequencies. Thus, this method suffers from the serious trade-off between accuracy and spatial resolution.

4. Proposed Method

To overcome the difficulty described above, this paper introduces a novel method for estimating height change, which employs multiple band-divided SAR images and their coherence functions to resolves the above ambiguity described in Sect. 2. To maintain the robustness of height estimation avoiding spatial averaging, this method focuses on the frequency characteristic of the multiple phases obtained by the multiple coherence functions. First, the multiple band-divided data are generated so that all data have the same frequency band but different center frequency denoted $f_{c,n}$

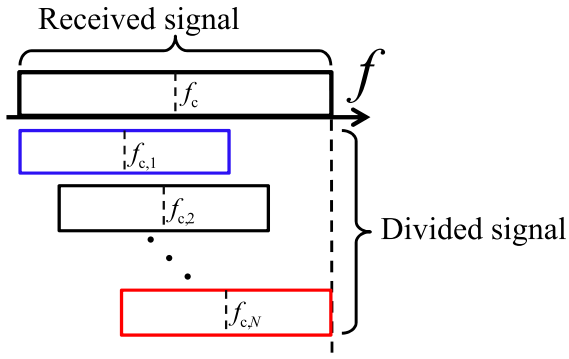

Fig. 4 Scheme for generating the data with multiple frequency bands.

($n = 1,\ldots,N$), where N is the total number of divided frequency bands. Figure 4 shows the scheme for generating the data with multiple frequency bands. Second, the SAR images before and after the change event are generated for each frequency band as $s_1(x,y;f_{c,n})$ and $s_2(x,y;f_{c,n})$, respectively. Third, this method calculates the coherence function using $s_1(x,y;f_{c,n})$ and $s_2(x,y;f_{c,n})$. The phase of this coherence to the amount of height change $\Delta z_{\mathrm{obs}}(x,y;f_{c,n})$ using Eq. (2). To resolve the ambiguity of height estimation, the optimum height change amount $\Delta\hat{z}_{\mathrm{prop}}(x,y)$ is calculated as,

$$\Delta\hat{z}_{\mathrm{prop}}(x,y) = \underset{|\Delta z_{\mathrm{est}}|\le\Delta z_{\max}}{\operatorname{argmin}} \sum_{n=1}^{N} \min_{k} \left| \Delta z_{\mathrm{obs}}(x,y;f_{c,n}) - \left(\Delta z_{\mathrm{est}} + \frac{k\mathrm{c}}{2f_{c,n}\cos\theta(x,y)} \right) \right|^2, \tag{6}$$

where Δz_{est} is variable for the estimated height change, $\Delta z_{\max}$ denotes the investigated range of height estimation, which is set to a sufficiently large value. Figure 5 shows the fitting approach described by Eq. (6). In this figure, the actual height change Δz_{true} is set outside the ambiguity limit, which is denoted by the dashed line. In contrast, the observed height change $\Delta z_{\mathrm{obs}}(f_{c,n})$ should be included in the region $|\ \Delta z_{\mathrm{obs}}\ | \le \mathrm{c}/4f_{c,n}\cos\theta$ as in Eq. (3). In case (a), the height change is not correctly estimated because the curved line determined by the height change of interest does not completely match the actual data points. In case (b), the height change is correctly estimated by completely adjusting the curved line to the data points. While the band-divided data are not completely independent of each other, it is expected that their robustness against phase fluctuation can be enhanced by employing multiple frequency data points.

Finally, the actual procedure of the proposed method is summarized as follows.

Step 1) Received signals are divided into N frequency bands with different center frequencies.

Step 2) SAR images taken before and after the change event are generated in each frequency band as $s_1(x,y;f_{c,n})$ and $s_2(x,y;f_{c,n})$, where $n = 1,2,\cdots,N$.

Step 3 Position adjustment between $s_1(x,y;f_{c,n})$ and $s_2(x,y;f_{c,n})$ is carried out for each center frequency, so that the output of local cross-correlation of these two

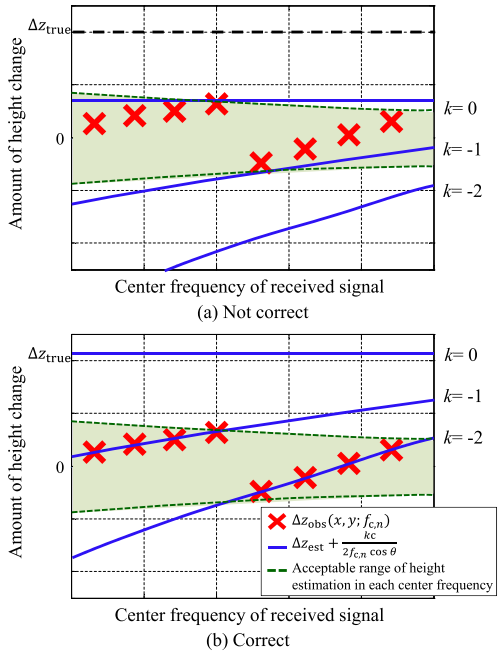

Fig. 5 Fitting approach for height change estimation with multiple frequency bands. (Case (a): Not correctly estimated, case(b): Correctly estimated)

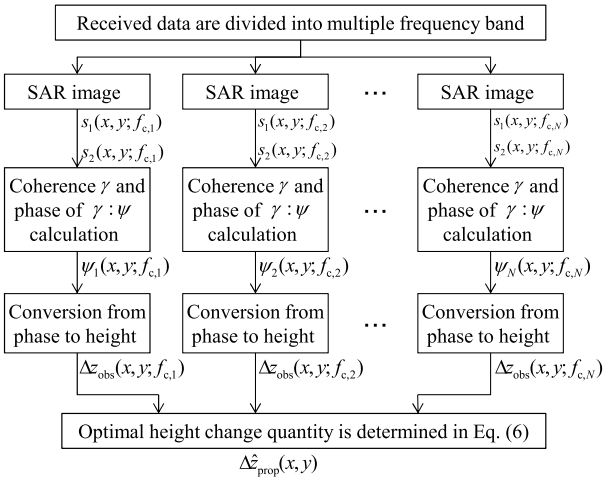

Fig. 6 Flowchart of the proposed method.

images becomes maximum. The window size of the local cross-correlation is empirically determined.

Step 4) Coherence function $\gamma_n(x, y; f_{c,n})$ is calculated from $s_1(x, y; f_{c,n})$ and $s_2(x, y; f_{c,n})$, and the phase of $\gamma_n(x, y; f_{c,n})$ as $\psi_n(x, y; f_{c,n})$ is also calculated.

Step 5) The height change is determined using Eqs. (2) and (6) with $\Delta z_{obs}(x, y; f_{c,n})$ obtained from $\psi_n(x, y; f_{c,n})$.

Figure 6 shows the flowchart of the proposed method.

5. Performance Evaluation

This section presents performance evaluations of the proposed and conventional methods employing numerical simulation and an experiment. First, we describe the observation and target model commonly used in the numerical simulation and experiment. Here, this simulation assumes a typical X-band observation model, where the slant range resolution is around 1 m (corresponding to 300 MHz bandwidth) and the center frequency is around 10 GHz. To adjust the possible experimental setup described in the following section, a 1/100 downscaled model for geometry and range resolution is adopted. However, with regard to the center frequency of the transmitted signal, it is difficult to adjust it to a realistic value (THz frequency required in 1/100 model) because of the limitation of the experimental device, and a 1/3 downscale model was then used. The minimum and maximum frequencies are $f_{min} = 26$ GHz and $f_{max} = 40$ GHz, respectively. The synthetic aperture length is 1.6 m and $z_0 = 0.914$ m. Here, the conventional method uses the dual-divided 8 GHz bandwidths with the center frequencies 30 GHz and 36 GHz, respectively. On the contrary, in the proposed method, the number of divided frequency bands N is 7, where each bandwidth of the received signal is 8 GHz and the interval of the center frequency (namely $f_{c,n+1} - f_{c,n}$) is 1 GHz. Then, the nominal range resolution in the both method is estimated as 18.75 mm. The off-nadir angle θ is set to 50° at the center of the observation line. The actual height change is given as,

$$\Delta z_{true}(x, y) = \begin{cases} \Delta z_t, & (x \geq 0) \\ 0. & (x < 0) \end{cases} \tag{7}$$

5.1 Numerical Simulation

This subsection describes the performance evaluation in a numerical simulation using the aforementioned model. A rough surface target is approximated as an aggregate of point targets. The signal received from these scattering points for each antenna location$(x, 0, z_0)$ is calculated as $S(x, f)$ [8]

$$S(x, f) = \begin{cases} \sum_{m=0}^{N_s-1} \frac{1}{R^2(x,m)} \exp\left[-j4\pi \frac{f}{c} R(x, m)\right], & (f_{min} \leq f \leq f_{max}) \\ 0, & (\text{otherwise}) \end{cases} \tag{8}$$

where N_s denotes the total number of scattering points. f_{min} and f_{max} are the minimum and maximum frequencies, respectively. c is the speed of radio waves in air. $R(x, m) = \sqrt{(x - x_m)^2 + y_m^2 + (z_0 - z_m)^2}$, where (x_m, y_m, z_m) is the location of a target point. A Hamming window is applied for range-sidelobe suppression. The SAR image is then reconstructed using the back projection algorithm [9]. Here, the target exists on the area that $-40\,\text{cm} \leq x \leq 40\,\text{cm}$ and $85\,\text{cm} \leq y \leq 135\,\text{cm}$, and its surface roughness is around ±0.1 mm. For investigation of a noisy case, white Gaussian noise is added to the observation data. The SNR is determined as the ratio of peak instantaneous signal power to the average noise power in the received signal.

The upper and lower sides of Fig. 7 show the estimated

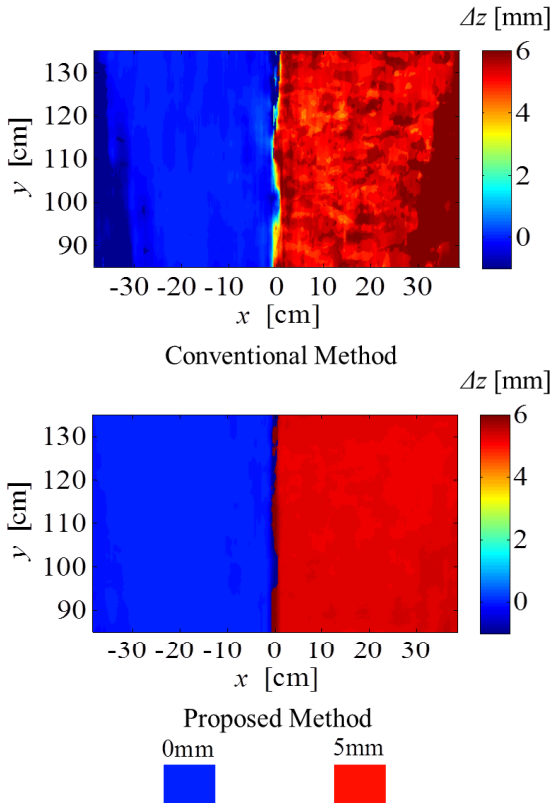

Fig. 7 Estimated distribution of the height change Δz_t=5 mm, obtained by each method (upper: Conventional, lower: Proposed) at noiseless situation.

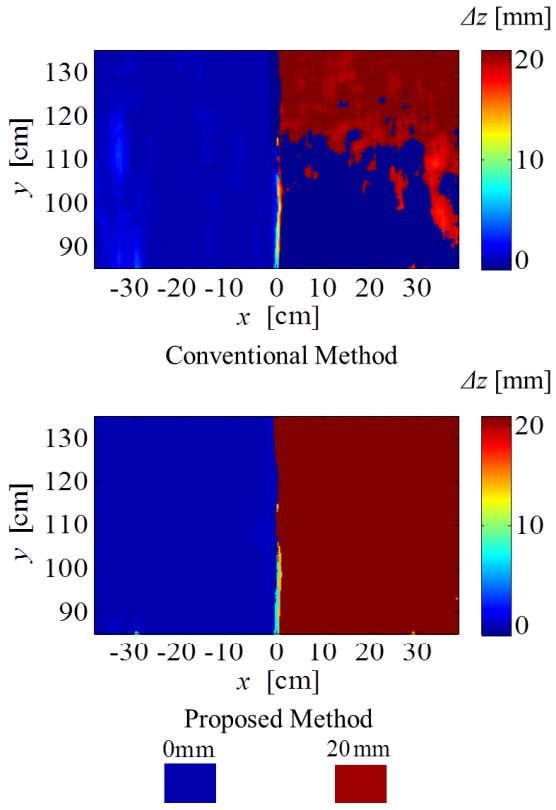

Fig. 8 Estimated distribution of the height change Δz_t=20 mm, obtained by each method (upper: Conventional, lower: Proposed) at noiseless situation.

height change distributions obtained with the conventional and proposed methods, respectively, in a noiseless situation, where $\Delta z_t = 5$ mm. Here, the conventional method does not employ spatial averaging regarding the standard of fairness. The correlation length(L) of the coherent function is set to 10 times the spatial resolution of the SAR image in both methods. The results show that the height change distribution can be accurately reconstructed by the proposed method, while the conventional method hardly obtains sufficient accuracy in suffering from phase fluctuations associated with noise. Here, we introduce an evaluation value for assessing the ambiguity resolution, whose condition is determined as

$$| \Delta z_{\text{true}} - \Delta \hat{z}_{\text{est}} | < \frac{c}{4 f_c \cos\theta}, \tag{9}$$

where $\Delta \hat{z}_{\text{est}}$ is the estimated height change amount for each method. The probability of ambiguity resolution of the conventional method is 97.9%, and that of the proposed method is 98.0%. In addition, the estimation accuracy is quantitatively assessed below. Here, we confirm that the probabilistic distribution of the error in height change for each method is far from that of a Gaussian distribution. To deal with such an error distribution appropriately, the median error and inter quartile range (IQR) are employed in assessing the bias error and its fluctuation. The median error in the height estimation is 0.02 mm for the conventional method and 0.02 mm for the proposed method. The IQR is 0.55 mm and 0.27 mm for the conventional and proposed methods, respectively. These results quantitatively demonstrate the effectiveness of the proposed method in terms of the accuracy of the height change estimation.

Furthermore, Fig. 8 shows the estimated height change distributions in the situation Δz_t=20 mm which is largely beyond the ambiguity determined in Eq. (3) for all center frequencies. The probability of ambiguity resolution for the conventional method is 70.9% and that for the proposed method is 93.6%. The median error in the height estimation is −0.02 mm for the conventional method and 0.05 mm for the proposed method.

The IQR is 23.24 mm and 1.16 mm in the conventional and proposed methods, respectively. In this case, the accuracy of the height change estimation reduces comparably. We consider that this is because the phase interference becomes more severe due to increasing the height change amount.

To validate the robustness of the proposed method, the evaluation of several height changes in noisy situation, that received data are contaminated by additional Gaussian white noises, is investigated. Figures 9 and 10 show the estimated height change distributions for $\Delta z_t = 5$ mm and $\Delta z_t = 20$ mm, respectively, where SNR=20 dB. These figures demonstrate that, in both cases, the proposed method suffers less from accuracy degradation than the conventional

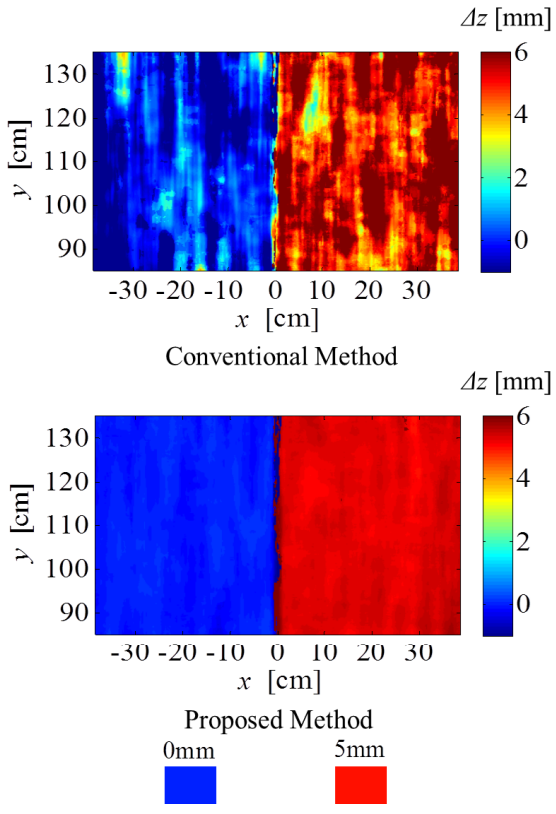

Fig. 9 Estimated distribution of the height change Δz_t = 5 mm, obtained by each method (upper: Conventional, lower: Proposed). SNR = 20 dB.

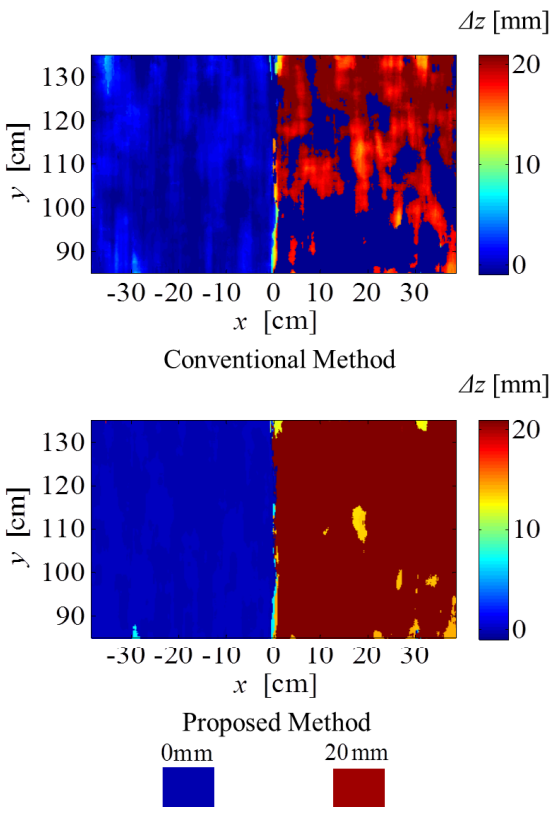

Fig. 10 Estimated distribution of the height change Δz_t=20 mm, obtained by each method (upper: Conventional, lower: Proposed). SNR = 20 dB.

method. This is because while the conventional method remarkably expands the non-ambiguity region, the accuracy of the method fatally degrades in the noisy situation owing to enhanced the phase fluctuation due to the differencing operation of each phase. From a statistical view point, Figures 11, 12 and 13 show the probability of ambiguity resolution, the median error and the IQR of height change estimation versus SNR, respectively, where Δz_t = 5 mm, Δz_t = 10 mm and Δz_t = 20 mm. The obtained results demonstrate that the proposed method estimates height more accurately, especially in terms of the error fluctuation denoted by the IQR, while the ambiguity resolution of the method significantly remains at almost the same level as that of the conventional method. This is mainly due to the proposed method resolving ambiguity by exploiting the multiple phases obtained from the multiple frequency bands. Besides, we confirmed that the proposed method offers almost same results, when the number of frequency bands is increasing such as 14 or 21. This is because each received data divided by smaller frequency interval include little independent information among neighbouring bands, since most part of frequency bands are overlapped in such case.

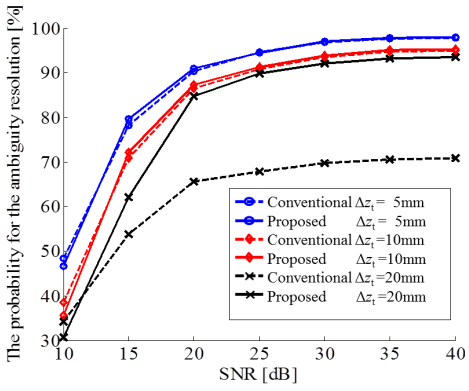

Fig. 11 The probability for the ambiguity resolution in each SNR and height change Δz_t.

5.2 Experiment

This subsection investigates the estimation of height change using experimental data. Figures 14 and 15 show the system model of the experiment and the scene of the experimental environment, respectively. The 3 dB beam width of each horn antenna is 27 degrees, and the interval between the transmitting and receiving antennas is 48 mm. On the transmitter side, a 20 dB amplifier is inserted to obtain a sufficient echo from the targets. The received data at each frequency are acquired by a vector network analyzer (VNA). Both the transmitting and receiving polarizations are a linear in the direction of y-z plane, i.e., vertical polarization. To adjust the possible experimental setup, a 1/100 down-

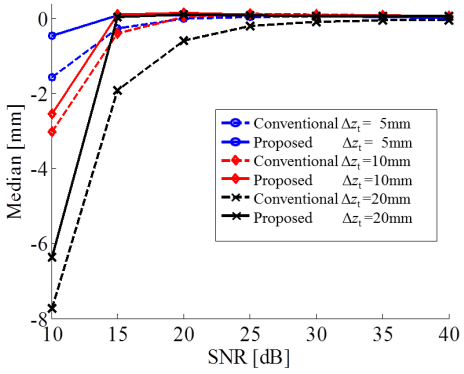

Fig. 12 The median error in each SNR and height change Δz_t.

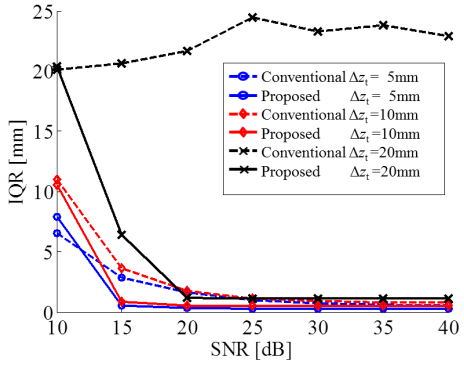

Fig. 13 The inter quartile range in each SNR and height change Δz_t.

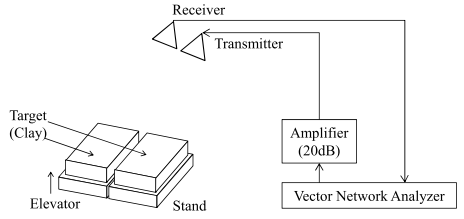

Fig. 14 System model of the experiment.

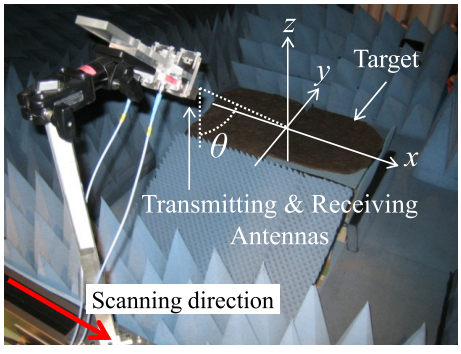

Fig. 15 Scene of the experimental environment.

scaled model of the target, geometry and spatial resolution is adopted, because an X-band radar system is assumed in this study, where the spatial resolution is around 2 m and the center frequency is around 10 GHz. A clay target with a rough surface, width of 800 mm, depth of 500 mm and thickness of 100 mm, and surface roughness around ±1 mm is chosen. A height change has added to the target in the area $x > 0$ using a screw lift. The accuracy of the height change is estimated as better than 0.5 mm. Figures 16 and 18 show the estimated height change distributions obtained by the conventional and proposed methods, respectively. Here, SNR=41 dB. These figures visually indicate that the proposed method provides a more accurate estimation of height change, even in the experimental environment for a similar to that discussed for the numerical simulation. Tables 1 and 2 summarize the probability of ambiguity resolution, the median error and the IQR of the height change estimation for the conventional and proposed methods, respectively. These tables quantitatively demonstrate that the proposed method can improve the IQR for the height change estimation (i.e., less fluctuation in the height change estimation) without degrading the ambiguity resolution performance compared with the conventional method.

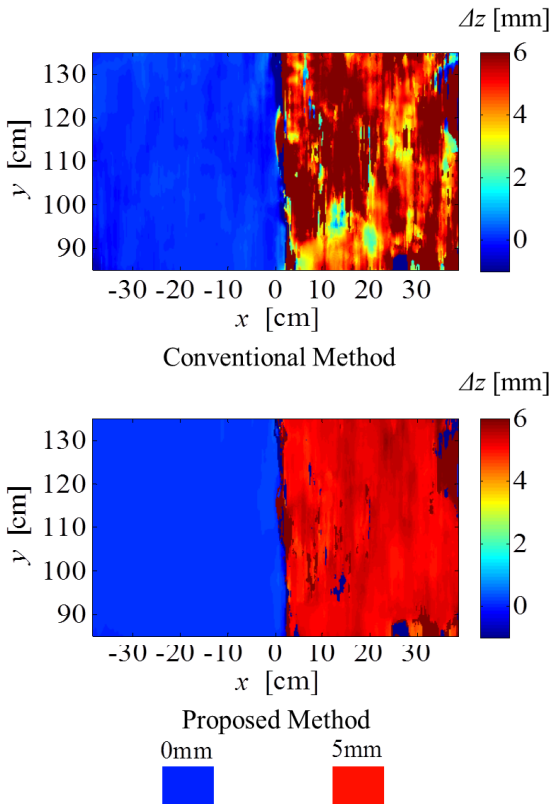

Fig. 16 Estimated distribution of the height change $\Delta z_t = 5$ mm, obtained by each method in experiment (upper: Conventional, lower: Proposed).

Table 1 The results of the experiment by the conventional method.

Δz_t [mm]	Probability [%]	Median of error [mm]	IQR [mm]
5	89.7	0.13	0.49
10	86.4	0.07	1.98
20	69.4	−0.15	5.47

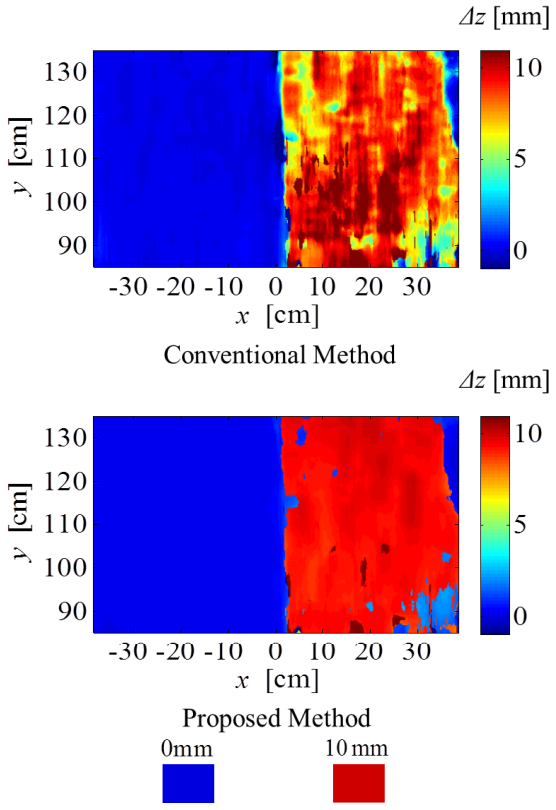

Fig. 17 Estimated distribution of the height change $\Delta z_t = 10\,\text{mm}$, obtained by each method in experiment (upper: Conventional, lower: Proposed).

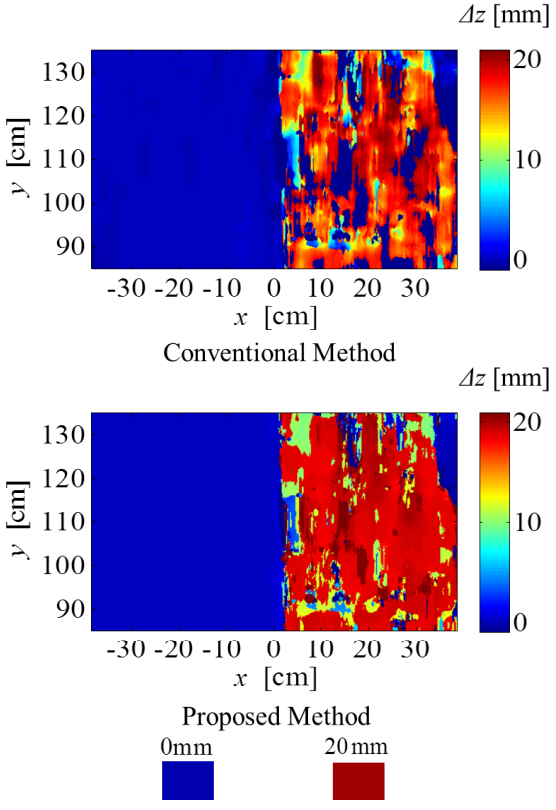

Fig. 18 Estimated distribution of the height change $\Delta z_t = 20\,\text{mm}$, obtained by each method in experiment (upper: Conventional, lower: Proposed).

Table 2 The results of the experiment by the proposed method.

Δz_t [mm]	Probability [%]	Median of error [mm]	IQR [mm]
5	90.2	0.16	0.1
10	87.7	0.09	0.84
20	78.1	0.16	1.61

5.3 Change Detection Performance in Experiment

As described in Sect. 1, as an advantage over InSAR measurements, it maintains its capability to detect change using the CCD observation model. In this subsection, we investigate its performance in such instances using experimental data to validate the above discussion. We have also proposed an accurate means of detecting change exploiting the phase of the coherence function $\gamma(x, y)$ calculated in Eq. (1) [10]. While major CCD methods employ the norm of $\gamma(x, y)$ for change detection, reports [10] demonstrate that the phase of $\gamma(x, y)$ is also useful to accurately measure change, especially for those situations assumed in this paper, i. e., a target surface that is uniformaly raised or sunken over a large area. This improved index is formulated as

$$\beta(x, y) = |1 - \gamma(x, y)\, \gamma_{\text{bias}}|\,, \tag{10}$$

where the compensation coefficient γ_{bias} is obtained from

$$\gamma_{\text{bias}} = \frac{\sum_{i=0}^{N_x-1} \sum_{j=0}^{N_y-1} \left|\gamma(x_i, y_j)\right| \gamma(x_i, y_j)}{\left|\sum_{i=0}^{N_x-1} \sum_{j=0}^{N_y-1} \left|\gamma(x_i, y_j)\right| \gamma(x_i, y_j)\right|}, \tag{11}$$

Here N_x and N_y denote the total numbers of samples for the x and y axes, respectively. This compensation coefficient solves the bias of the phase of $\gamma(x, y)$ caused by the mismatch among sensor orbits. Equation (10) assesses the Euclidean distance on the Gaussian plane from $(1, 0)$, that is, $s_1(x, y) = s_2(x, y)$ holds. The left column of images in Fig. 19 presents the spatial distribution of $\gamma(x, y)$ at various heights, (a) $\Delta z_t = 5\,\text{mm}$, (b) $\Delta z_t = 10\,\text{mm}$ and (c) $\Delta z_t = 20\,\text{mm}$. Althogh the norm of $\gamma(x, y)$ are degraded in the height change area in each case, these degradations are less noticeable, especially for the 10 mm height change. This is because, with uniform height changes, a phase difference mainly occurs in $\gamma(x, y)$. The images in the right column of Fig. 19 show the distribution of $\gamma(x, y)$ and detection boundary using $|\gamma(x, y)|$ and $\beta(x, y)$ for each case, where each boundary is adjusted to maintain a probability for false alarms of $P_{\text{fa}} = 10^{-3}$. The red and blue points in these figures represent $\gamma(x, y)$ generated by "changed" and "unchanged" areas. As shown in these figures, the index $\beta(x, y)$ is more suitable in detecting change by consider-

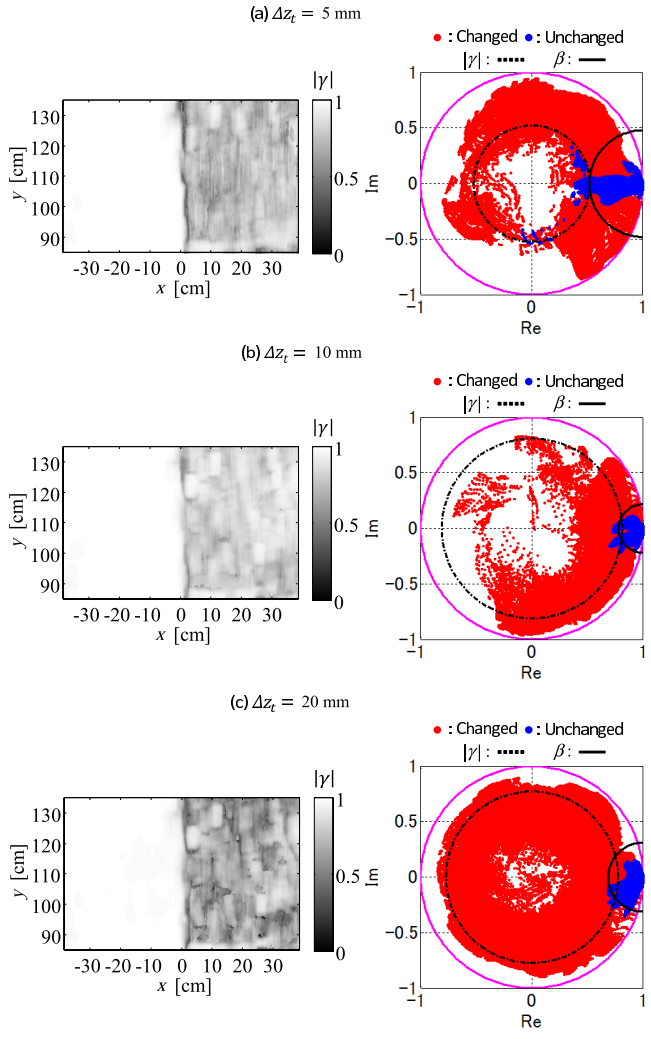

Fig. 19 Estimated distribution of $|\gamma(x, y)|$ (left) and $\gamma(x, y)$ distribution on Gaussian plane (right) for each height change case as (a): Δz_t = 5 mm, (b): Δz_t = 10 mm and (c): Δz_t = 20 mm.

ing the phase rotation of γ without its norm degradation. Finally, Fig. 20 shows the receiver operating characteristic (ROC) in change detection using $\beta(x, y)$ for each change in height. As shown in this figure, an accurate detection of change is accomplished by focusing the phase of $\gamma(x, y)$. This also verifies that the proposed method is applicable to the original CCD issue by simultaneously offering significant information about the amount of height change.

As a final remark, we assume the observation model of 1/100 th scale down model of the X-band radar except for the center frequency. Then, the 20 mm height change, regarded as the maximum range change in the numerical or experimental investigations, is roughly converted to 200 cm height change in the actual scenario, and the propagation delay due to moisture vapor and the baseline accuracy (both of the order of cm) causes a relatively smaller impact for an actual height change estimation. However, the center frequency is only 1/3 of the actual measurement owing to performance limitations of the VNA. In real damage assessment, because much smaller center wavelengths are used compared with that assumed in this experiment, there is expected to be more difficulty in estimating height change because the local optimum in assessing the evaluation function in Eq. (6) would increase for smaller center wavelength, thus causing difficulty in finding the global optimum. We then need a more efficient optimization scheme to obtain actual changes in height in real scenarios.

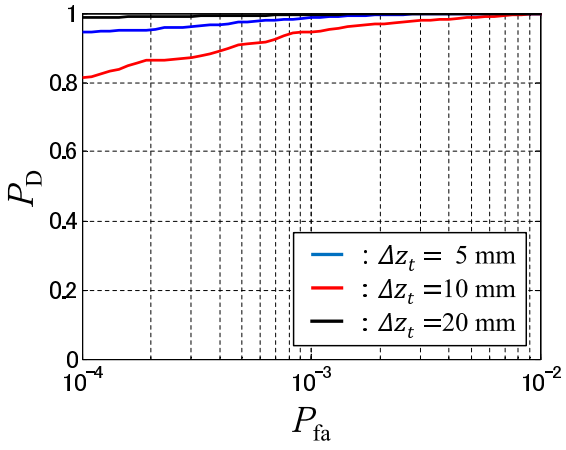

Fig. 20 Receiver operating characteristic (ROC) for each height change case by using the change detection index $\beta(x, y)$.

6. Conclusion

This paper proposed a novel method for accurately estimating height change that employs the coherence phases obtained from multiple band-divided SAR images. This method focuses on the frequency characteristic obtained by the multiple band-divided coherence function, and offers enhanced height change estimation accuracy while maintaining the same level of ambiguity resolution offered by the conventional scheme. Both numerical simulations including a noisy case and experimental data verified that the proposed method offers more accurate height change estimation while retaining a high probability of resolving ambiguity. Furthermore, another performance as surface change detection has been demonstrated using not only the norm of γ but also the phase of γ, which cannot be assessed by the InSAR observation model.

References

[1] W.M. Brown, "Synthetic aperture radar," IEEE Trans. Aerosp. Electron. Syst., vol.AES-3, pp.217–229, March 1967.
[2] R. Goodman, S. Tummala, and W. Carrara, "Issues in ultrawideband, widebeam SAR image formation," Proc. IEEE International Radar Conf., pp.479–485, May 1995.
[3] R. Touzi, A. Lopes, J. Bruniquel, and P.W. Vachon, "Coherence estimation for SAR imagery," IEEE Trans. Geosci. Remote Sens., vol.37, no.1, pp.135–149, Jan. 1999.
[4] P.A. Rosen, S. Hensley, I.R. Joughin, F.K. Li, S.N. Madsen, E. Rodriguez, and R.M. Goldstein, "Synthetic aperture radar interferometry," Proc. IEEE, vol.88, no.3, pp.333–382, March 2000.
[5] S. Sauer, L, Ferro-Famil, A. Reigber, and E. Pottier, "Three-

dimensional imaging and scattering mechanism estimation over urban scenes using dual-baseline polarimetric InSAR observations at L-band," IEEE Trans. Geosci. Remote Sens., vol.49, no.11, pp.4616–4629, Nov. 2011.

[6] K.A. Câmara De Macedo, C. Wimmer, T.L.M. Barreto, D. Lübeck, J.R. Moreira, L.M.L. Rabaco, and W.J. de Oliveira, "Long-term airborne DInSAR measurements at X-and P-Bands: A case study on the application of surveying geohazard threats to pipelines," IEEE J. Sel. Topics in Applied Earth Observations & Remote Sensing, vol.5, no.3, pp.990–1005, June 2012.

[7] T. Hoshino, S. Kidera, and T. Kirimoto, "Height change estimation algorithm based on frequency interferometer of coherence function in CCD model," Proc. IEICE Gen. Conf., B-2-43, March 2011 (in Japanese).

[8] L. Tsang, J.A. Kong, K.-H. Ding, and C.O. Ao, Scattering of Electromagnetic Waves: Numerical Simulations, pp.581–590, Wiley, New York, 2001.

[9] L.M.H. Ulander, H. Hellsten, and G. Stenstrom, "Synthetic-aperture radar processing using fast factorized back-projection," IEEE Trans. Aerosp. Electron. Syst., vol.39, no.3, pp.760–776, July 2003.

[10] T. Hoshino, S. Kidera, and T Kirimoto, "Accurate Surface Change Detection Method using Phase of Coherence Function on SAR Imagery," IEICE Trans. Commun., vol.E95-B, no.1, pp.263–270, Jan. 2012.

Ryo Nakamata received his B.E. degrees in Electronic Engineering from University of Electro-Communications in 2011 and M.M. degree at the Graduate School of Informatics and Engineering, University of Electro-Communications in 2013. He joined Sigmatron Co., Ltd. in 2013.

Ryo Oyama received his B.E. degrees in Electronic Engineering from University of Electro-Communications in 2013. He is currently studying M.E. degree at the Graduate School of Informatics and Engineering, University of Electro-Communications. His current research interest is advanced radar signal processing of SAR application.

Shouhei Kidera received his B.E. degree in Electrical and Electronic Engineering from Kyoto University in 2003 and M.I. and Ph.D. degrees in Informatics from Kyoto University in 2005 and 2007, respectively. He is an assistant professor in Graduate School of Informatics and Engineering, University of Electro-Communications, Japan. His current research interest is in advanced radar signal processing or electromagnetic inverse scattering issue for ultra wideband (UWB) sensor. He was awarded Young Scientist's Prize in 2013 by the Japanese Minister of Education, Culture, Sports, Science and Technology (MEXT). He is a member of the Institute of Electrical and Electronics Engineering (IEEE) and the Institute of Electrical Engineering of Japan (IEEJ).

Tetsuo Kirimoto received the B.S. and M.S. and Ph.D. degrees in Communication Engineering from Osaka University in 1976, 1978 and 1995, respectively. During 1978–2003 he stayed in Mitsubishi Electric Corp. to study radar signal processing. From 1982 to 1983, he stayed as a visiting scientist at the Remote Sensing Laboratory of the University of Kansas. From 2003 to 2007, he joined the University of Kitakyushu as a Professor. Since 2007, he has been with the University of Electro-Communications, where he is a Professor at the Graduate School of Informatics and Engineering. His current study interests include digital signal processing and its application to various sensor systems. Prof. Kirimoto is a senior member of IEEE and a member of SICE (The Society of Instrument and Control Engineers) of Japan.